

Phonon state tomography of electron correlation dynamics in optically excited solids

M. Moroder,¹ M. Mitrano,² U. Schollwöck,¹ S. Paeckel,^{1,*} and J. Sous^{3,†}

¹*Department of Physics, Arnold Sommerfeld Center for Theoretical Physics (ASC),
Munich Center for Quantum Science and Technology (MCQST),
Ludwig-Maximilians-Universität München, 80333 München, Germany*

²*Department of Physics, Harvard University, Cambridge, Massachusetts 02138, USA*

³*Department of Chemistry and Biochemistry, University of California San Diego, La Jolla, California 92093, USA*

We introduce phonon state tomography (PST) as a diagnostic probe of electron dynamics in solids whose phonons are optically excited by a laser pulse at an initial time. Using a projected-purified matrix-product states (PP-MPS) algorithm, PST decomposes the exact correlated electron-phonon wavefunction into contributions from purely electronic states corresponding to statistically typical configurations of the optically accessible phononic response, enabling a ‘tomographic’ reconstruction of the electronic dynamics generated by the phonons. Thus, PST may be used to diagnose electronic behavior in experiments that access only the phonon response, such as thermal diffuse x-ray and electron scattering. To demonstrate the usefulness of PST, we study the dynamics of a metal whose infrared phonons are excited by an optical pulse at initial time and use it to simulate the sample-averaged momentum-resolved phonon occupancy as would be measured experimentally and accurately reconstruct the electronic double occupancy and staggered magnetization. We also use PST to analyze the influence of different pulse shapes on the light-induced enhancement and suppression of electronic correlations.

Optical driving of quantum materials has opened a door for engineering and controlling novel electronic states of matter, with a prime example being the generation of non-equilibrium superconducting states [1–9] and emergent Floquet phases [10–13]. One important class of experiments involves the optical excitation of specific phonons that couple strongly to the electronic states [14–20]. These infrared-active phonons inherit the dipole character of light which means that the coupling between the electrons and photoexcited phonons is governed by dipole selection rules. As a result, in centrosymmetric crystals, lattice nonlinearities govern the light-induced dynamics giving rise to novel behavior inaccessible in equilibrium where nonlinear couplings are subdominant fluctuations [21].

Probing and interpreting this rich behavior in the post-pump dynamics is a rapidly growing area of research whose goal is to extract a reliable understanding of the light-induced energy transport and electronic correlations. Optical probes provide direct access to charge transport [2, 7]. However, accurate simulation of transport far away from equilibrium in strongly correlated electron-phonon systems remains a daunting challenge [21–29], complicating interpretation of experiments. Direct phonon probes such as x-ray diffuse scattering [30, 31] and electron scattering [32] provide access to the phononic response induced by coupling to the electrons. Here we present a matrix-product state (MPS)-based method, dubbed phonon state tomography (PST) (Fig. 1), to simulate the sample-averaged dynamics of the phonon distribution function as would be obtained in x-ray diffuse scattering and electron scattering experiments. PST enables us to represent the full electron-phonon wavefunction accurately in terms of electronic components associated with the experimentally

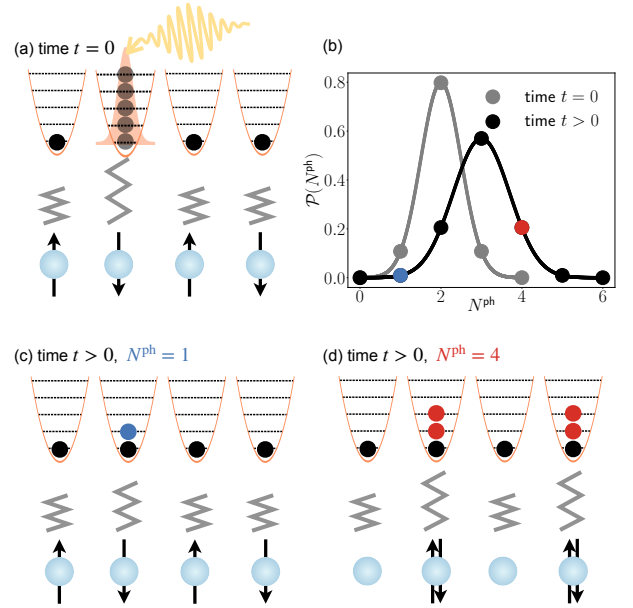


FIG. 1. Phonon state tomography (PST). (a) A metal whose electrons (blue spheres) couple locally to phonons (black dots) which are excited at $t = 0$ by a pump pulse. (b) The probability $\mathcal{P}(N^{\text{ph}})$ to find N^{ph} at initial and later times. (c) and (d) Schematic of the tomographic decomposition of the wavefunction for one and four phonon excitations, respectively.

measured phononic quantity, e.g. the sample-averaged momentum-resolved phonon occupation. Using this decomposition we can accurately reconstruct electronic correlation functions by sampling electronic contributions associated with the statistically typical phononic configurations inferred from the spatially resolved phonon density matrix. This means that PST can be used as a diagnostic tool to relate the experimentally obtained sample-averaged phonon response following various time

delays to the dynamics of electronic correlation functions, providing a *one-to-one relation* between the statistically measured phononic response and the underlying electronic behavior. Once matched to experimental measurements, PST can be used to tomographically reconstruct the electronic correlations without need for the full exact electron-phonon wavefunction. The tomographic decomposition of the electron-phonon wavefunction and sampling over statistically weighted electronic states is made possible thanks to a new class of projected-purified matrix-product states (PP-MPS) methods [33, 34] which enables efficient computation of the spatially resolved global and local phonon reduced density matrices of the coupled electron-phonon system.

Given this, PST may provide insights into the microscopic physics of materials probed in experiments that access the frequency, damping, occupation number, and couplings to other degrees of freedom of the optically excited phonon subsystem interrogated with multiple time-resolved probes, such as infrared and Raman spectroscopy, x-ray, and electron scattering. This may shed light into the mechanism behind dynamically-enhanced superconductivity in the copper oxides [35, 36] and organic materials [2, 37], as well as of light-induced ferroelectricity [38] and high-temperature ferromagnetism [39]. In these materials, specific phonon resonances in the dynamical optical response [40, 41] as well as signatures of structural distortions due to nonlinearities [42, 43] highlight the significant role phonons play in the dynamics.

A particularly intriguing class of experiments are those based on diffuse x-ray and electron scattering, in which the scattering intensity is directly proportional to a weighted sum of phonon populations for different branches and at different momenta. In the first-order kinematical approximation [44], the diffuse scattering intensity I_S is given by

$$I_S \sim \sum_i \frac{1}{\omega_i(\mathbf{k})} \left(n_i(\mathbf{k}) + \frac{1}{2} \right) |F_i(\mathbf{k})|^2, \quad (1)$$

where $\omega_i(\mathbf{k})$, $F_i(\mathbf{k})$, and $n_i(\mathbf{k})$ are frequency, structure factor and occupation number of the i^{th} phonon branch at momentum \mathbf{k} . Given the Hamiltonian governing the electronic and phononic dynamics and their couplings, PST would enable simulation of I_S and reconstruction of associated electronic correlations, thus potentially enabling interpretation of the ultrafast electron diffraction and x-ray diffuse scattering on cuprate superconductors (e.g. $\text{Bi}_2\text{Sr}_2\text{CaCu}_2\text{O}_{8+\delta}$ and $\text{YBa}_2\text{Cu}_3\text{O}_{6+\delta}$) under resonant excitation of the c -axis apical oxygen distortions [40].

Phonon state tomography. Given the exact electron-phonon wavefunction, the idea behind PST is to draw samples of electronic states $|\psi^{\text{el}}(\mathbf{n}^{\text{ph}})\rangle$ associated with statistically typical phononic configurations labeled by

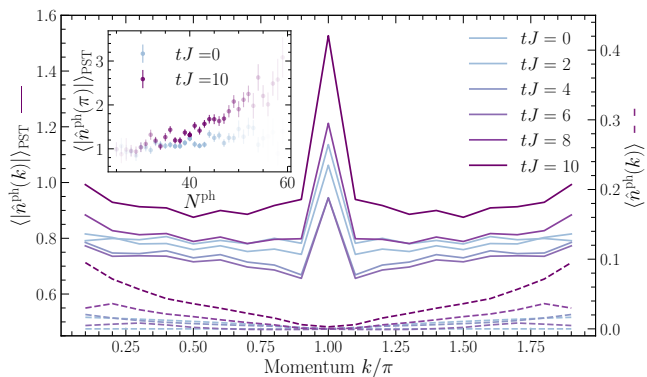


FIG. 2. Sample-averaged momentum-resolved amplitude of the phonon distribution function $\langle |\hat{n}^{\text{ph}}(k)| \rangle_{\text{PST}}$ from PST and the corresponding expectation value of the momentum-resolved phonon distribution function $\langle \hat{n}^{\text{ph}}(k) \rangle$ following different time delays. We decompose $\langle |\hat{n}^{\text{ph}}(\pi)| \rangle$ into contributions from different total phonon number sectors N^{ph} in the inset. The color intensity of the symbols indicates the fraction of all drawn samples found to have the corresponding value of N^{ph} . We used 3000 samples to construct this data. Error bars represent statistical errors corresponding to 1 standard deviation scaled by the inverse of the square root of the number of samples.

their global spatially-resolved phonon occupation over the lattice $\mathbf{n}^{\text{ph}} = (n_1^{\text{ph}}, n_1^{\text{ph}}, \dots, n_L^{\text{ph}})$, where L is the system size. We thus decompose the electron-phonon wavefunction as

$$|\psi\rangle = \sum_{\{\mathbf{n}^{\text{ph}}\}} |\psi^{\text{el}}(\mathbf{n}^{\text{ph}})\rangle \otimes \left(\sqrt{p(\mathbf{n}^{\text{ph}})} |\mathbf{n}^{\text{ph}}\rangle \right), \quad (2)$$

where $|\psi^{\text{el}}(\mathbf{n}^{\text{ph}})\rangle \in \mathcal{H}^{\text{el}}$ are normalized electronic states with span in the electronic Hilbert space \mathcal{H}^{el} , $|\mathbf{n}^{\text{ph}}\rangle \in \mathcal{H}^{\text{ph}}$ are phonon number states with span in the phononic Hilbert space \mathcal{H}^{ph} , and $p(\mathbf{n}^{\text{ph}})$ is the probability of finding the phonon configuration \mathbf{n}^{ph} in the state $|\psi\rangle$. We represent $|\psi\rangle$ as a MPS [45–48]. We generalize the perfect sampling scheme (PSS) employed in snapshot techniques used in the study of ultracold atoms [49–55] to draw phonon configurations \mathbf{n}^{ph} distributed according to $p(\mathbf{n}^{\text{ph}})$ and the associated electronic states $|\psi^{\text{el}}(\mathbf{n}^{\text{ph}})\rangle$. The sampling is performed by successively decomposing $p(\mathbf{n}^{\text{ph}})$ into the probability over a given lattice site conditioned on the probability over the remaining sites: $p(\mathbf{n}^{\text{ph}}) = p(n_j^{\text{ph}})p(\mathbf{n}^{\text{ph}} \setminus n_j^{\text{ph}} | n_j^{\text{ph}})$ (where $\mathbf{n}^{\text{ph}} \setminus n_j^{\text{ph}}$ is the set of occupations associated with all sites except site j), see supplemental materials [56] for details.

PST of an optically pumped metal. To demonstrate the power of the PST, we simulate the dynamics of the sample-averaged momentum-resolved phonon distribution function and reconstruct the associated electronic correlations of a one-dimensional metal whose phonons are excited by a light pulse at initial time. This system

is governed by the Hamiltonian [21, 24]

$$\hat{H} = -J \underbrace{\sum_{j=1}^L \sum_{\sigma=\uparrow,\downarrow} \left(\hat{c}_{j,\sigma}^\dagger \hat{c}_{j+1,\sigma} + \text{h.c.} \right)}_{\hat{H}_{\text{el}}} + \underbrace{\omega \sum_{j=1}^L \left(\hat{b}_j^\dagger \hat{b}_j + \frac{1}{2} \right)}_{\hat{H}_{\text{ph}}} + \underbrace{g \sum_{j=1}^L (\hat{n}_j - 1) \left(\hat{b}_j^\dagger + \hat{b}_j \right)^2}_{\hat{H}_{\text{el-ph}}}. \quad (3)$$

Here, electrons with spin σ and hopping amplitude J are quadratically coupled with coupling coefficient g to Einstein oscillators with frequency ω on a chain with size L . This nonlinear coupling follows from the fact that optically accessible phonons are long-wavelength dipole modes that cannot couple linearly to electrons in the presence of inversion symmetry [15, 16, 57]. We choose a very small value of g so that the initial equilibrium state is essentially indistinguishable from a metal of free fermions in a product state with the vacuum of the phonons. We simulate the dynamics following the application an impulsive spatially homogeneous pump pulse $\hat{A}^c \equiv \hat{D}(\alpha) = \prod_i \hat{d}_i(\alpha) \equiv \prod_j e^{\alpha \hat{b}_j^\dagger - \alpha^* \hat{b}_j}$ (α is the pump fluence) which coherently and uniformly displaces the oscillator on every site of the crystal. To simulate the dynamics we use a hybrid time-evolution scheme for the MPS combining global and local expansion techniques [58–62] and represent the phononic degrees of freedom with projected purification (PP) [33, 34], see supplemental materials [56] for details. In the following we consider a system size with $L = 20$ with $g/J = 0.07$, $\omega/J = \pi/10$ and $\alpha = \sqrt{2}$. We employ a local phonon Hilbert space dimension of up to $d^{\text{ph}} = 40$ which we verify to be sufficient to achieve convergence to the limit of the infinite phonon Hilbert space.

Sample-averaged momentum-resolved phonon distribution function. We use PST to simulate the experimental protocol used in measuring the sample-averaged momentum-resolved phonon distribution function. Phonon probes such as x-ray diffuse and electron scattering measure the momentum-resolved phonon distribution function for a given sample and statistically significant results are constructed by averaging over a sufficiently large number of samples. Experiments do not access the phase associated with the momentum-resolved phonon distribution function for a given sample, thus the sample-averaged momentum-resolved phonon occupation function corresponds to the sample-averaged amplitude of the Fourier-transformed spatially-resolved phonon distribution function measured for every given sample. We thus use PST to simulate the sample-averaged absolute value of the Fourier-transformed phonon occupation $\langle |\hat{n}^{\text{ph}}(k)| \rangle$ (which we henceforth refer to as $\langle |\hat{n}^{\text{ph}}(k)| \rangle_{\text{PST}}$). In Fig. 2, we show $\langle |\hat{n}^{\text{ph}}(k)| \rangle_{\text{PST}}$ and the expectation value of the phonon occupation in the exact

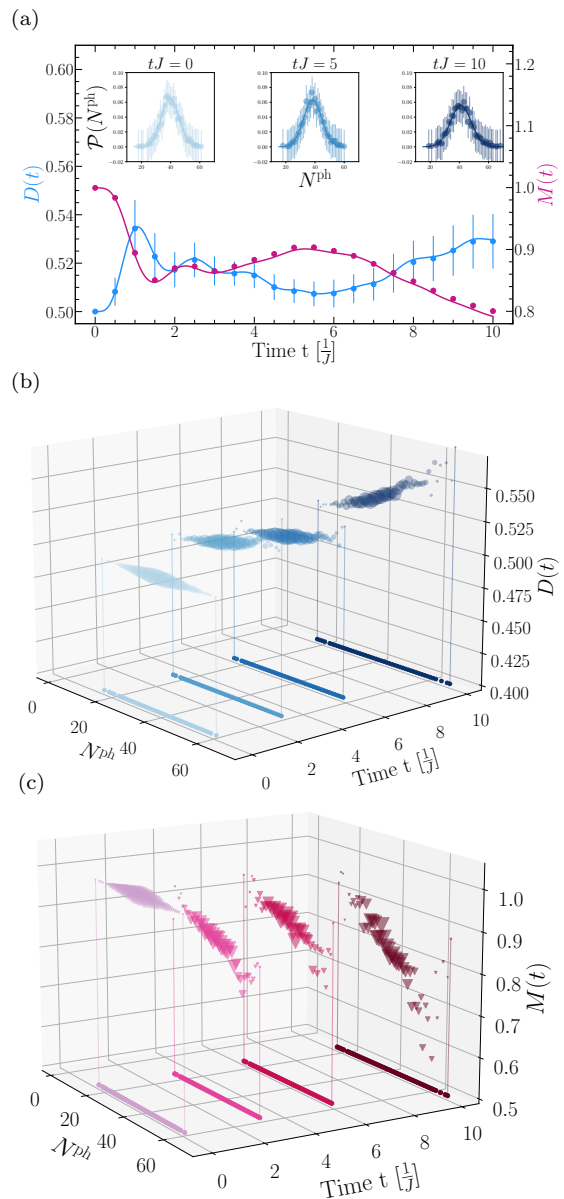


FIG. 3. Dynamics of electronic correlations reconstructed using PST. (a) The reconstructed charge double occupancy $D(t)$ (left axis) and staggered magnetization $M(t)$ (right axis) (symbols with error bars) are compared with the exact correlations (solid lines). In the inset, we show the sampled global phonon distribution function $\mathcal{P}(N^{\text{ph}})$ at different times. In panels (b) and (c) we obtain a decomposition of $D(t)$ and $M(t)$, respectively, into contributions from different total phonon number sectors N^{ph} . Here, the size of the symbols indicates the fraction of all drawn samples found to have the corresponding value of N^{ph} . We find that contributions from relatively large- N^{ph} sectors are the most important for reconstructing $D(t)$ and $M(t)$. The small dots at the bottom of panels (b) and (c) are projections onto the plane which serve as a guide for the eye. We have used 2000 samples in this figure. Error bars represent statistical errors corresponding to 1 standard deviation scaled by the inverse of the square root of the number of samples.

electron-phonon wavefunction $\langle \hat{n}^{\text{ph}}(k) \rangle$. Averaging the

amplitude of the occupation function over sample realizations *after* applying the Fourier transform provides qualitatively different information than that obtained from the exact expectation value of the phonon occupation containing the phase relation between different components of the full wavefunction. This is an important result because it means that access to the full electron-phonon wavefunction is *not* sufficient to directly interpret sampled-averaged momentum-resolved phononic observables obtained in experiments and that appropriately decomposing the full wavefunction into a suitable basis corresponding to the experimentally measured quantity, the momentum-resolved phonon occupation in this case, is essential. That is precisely what PST achieves.

An important feature in the simulated $\langle |\hat{n}^{\text{ph}}(k)| \rangle_{\text{PST}}$ is the appearance of a peak at $k = \pi$ absent in the exact expectation value of the phonon occupation. We understand this behavior qualitatively as follows. To construct a sample with a given total phonon number N^{ph} one samples over different phonon occupations whose sum adds up to N^{ph} ; these occur with probability given by the onsite local phonon distribution function (which is Poisson at initial time). This means that exciting different phonon numbers at different sites occurs with unequal probabilities (because the local distribution function is not uniform), leading to an overall inhomogeneity in the distribution of phonon states over the lattice. This manifests as a nearest-neighbor structure which gives rise to a peak at $k = \pi$ in the sample-averaged phonon occupation. Importantly, at initial time, just after the application of the pump, the Poisson distribution over phonon number states on each site means that low-lying phonon number states are more likely to be occupied with an average of $|\alpha|^2 = 2$ phonons excited on each site. At later times more phonons are excited in the course of the dynamics. Indeed this is what we observe numerically in the inset of Fig. 2 where we decompose $\langle |\hat{n}^{\text{ph}}(\pi)| \rangle_{\text{PST}}$ into contributions from sectors with total phonon number $N^{\text{ph}} \equiv \langle \sum_j \hat{n}_j^{\text{ph}} \rangle$ both at initial and late times. In the following, we will connect this observation to the analysis of electronic correlations.

Tomographically reconstructed electronic correlations. Given the tomographic representation of the wavefunction Eq. (2), we reconstruct the electronic double occupancy $D(t) = \frac{1}{L} \sum_{j=0}^{L-1} \langle (\hat{n}_j^d - \langle \hat{n}_j^d \rangle)^2 \rangle(t)$ ($\hat{n}_j^d = \hat{n}_{j,\uparrow} \hat{n}_{j,\downarrow}$) and the staggered magnetization $M(t) = \frac{1}{L} \sum_{j,l=0}^{L-1} (-1)^{j-l} \langle (\hat{s}_j^z - \langle \hat{s}_l^z \rangle)^2 \rangle(t)$ and show their dynamics in Fig. 3a. We observe evolution towards a state with a slight increase of the electronic double occupancy accompanied by suppression of the staggered magnetization consistent with the observations of Ref. [21]. Importantly, the tomographical reconstructed data (symbols with error bars) and the exact results (solid lines) are in perfect agreement, indicating that PST can accurately reconstruct electronic correlations. We find convergence

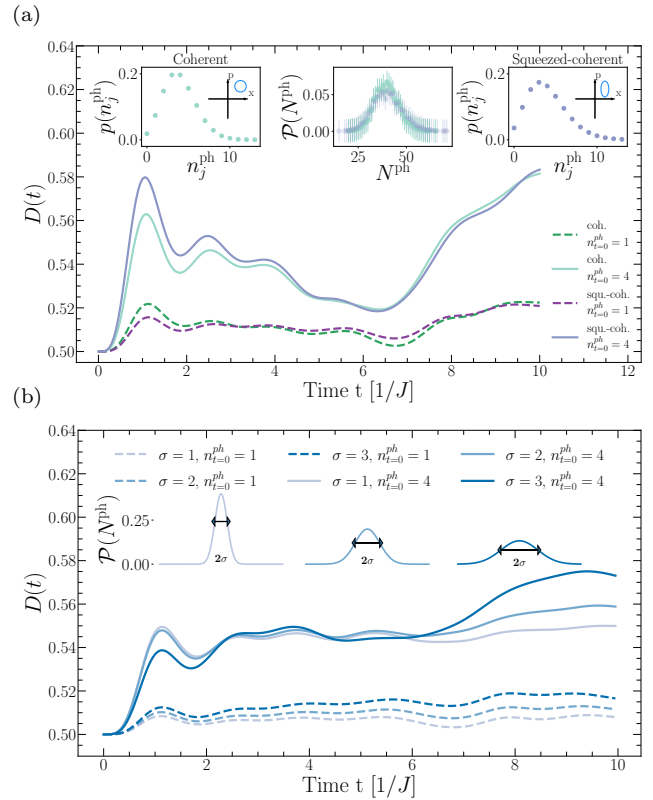


FIG. 4. Analysis of the effect of the pulse shape on the induced dynamics of charge double occupancy $D(t)$ obtained by constructing the phonon probability distribution $P(N^{\text{ph}})$ using PST. In (a) we compare the dynamics following the application of a coherent-exciting pulse \hat{A}^c with that following a squeezed-coherent-exciting pulse \hat{A}^{sc} , while in (b) we analyze the dynamics for different values of β following the application of a β -pulse \hat{A}^β . The left and right insets in (a) show the onsite local phonon probability distribution function over phonon number states for a coherent excitation (left) and a squeezed-coherent excitation (right), while the central inset shows the total phonon number distribution function for both pulses. (Note that the pump fluence corresponds to the expected value of n^{ph} given its probability distribution function $P(n^{\text{ph}})$). The dynamics following both pulses appear to be very similar, suggesting that it is controlled by $P(N^{\text{ph}})$. This is further corroborated in (b) where we find that the larger the width of $P(N^{\text{ph}})$, σ , the larger the induced double occupancy. We use $L = 10$ sites and 2000 samples in this figure.

to accurate results is possible for less than 2000 samples of phonon configurations, implying that while the exact electron-phonon wavefunction is exponentially large in the phonon Hilbert space (40^L), a reasonably small part of the phononic Hilbert space is all that is needed in order to fully quantify and faithfully reconstruct the electronic correlation dynamics. PST also allows us to decompose $D(t)$ and $M(t)$ into contributions associated with sectors with different total phonon number N^{ph} , which we study in Fig. 3b and Fig. 3c, finding that the dynamics of electronic correlations at later times is well dominated by contributions from total phonon number sectors with large value of N^{ph} accompanied by a slight increase

in the width of its distribution function $\mathcal{P}(N^{\text{ph}})$ (insets of Fig. 3a). Notably, we also find that the electronic double occupancy correlates with N^{ph} , while the staggered magnetization anticorrelates with N^{ph} . Combining all these observations, PST enables relating the formation of a $k = \pi$ peak in the sample-averaged phonon occupation driven by contributions from large- N^{ph} configurations to the evolution of electronic correlations.

Tomographic analysis of pulse shapes. The wavefunction decomposition obtained from PST indicates a significant dependence of the dynamics of electronic correlations on the population of high- N^{ph} configurations. This suggests a possibly controllable enhancement of electronic correlations using tailored optical pulses, as we demonstrate in the following. Besides \hat{A}^c , we consider $\hat{A}^{\text{sc}} = \prod_j \hat{d}_j(\alpha) e^{\frac{1}{2}(z^* \hat{b}_j^2 - z \hat{b}_j^{\dagger 2})}$ which generates squeezed-coherent phonon states with squeezing parameter z . This pulse shape enables control over the ratio between the standard deviation of the position and momentum operators $\Delta x / \Delta p$ at each site by varying z , therefore acts as a knob of control for tuning the width of the onsite local phonon distribution created by the pump (c.f. left and right insets of Fig. 4a). We also design an artificial pulse that depends on a single real parameter β which enables explicit control over the width of the global phonon distribution function $\mathcal{P}(N^{\text{ph}})$, we dub β -pulse

$$\hat{A}^\beta = \prod_j \left[\hat{b}_j^\dagger \right]^{n^{\text{ph}}} \left(\frac{\sqrt{1-2\beta^2}}{\sqrt{n^{\text{ph}}!}} + \frac{\beta \hat{b}_j^\dagger}{\sqrt{n^{\text{ph}}+1!}} + \frac{\beta \hat{b}_j}{\sqrt{n^{\text{ph}}-1!}} \right).$$

The generated initial global phonon distribution $\mathcal{P}(N_m^{\text{ph}}) = \sum_{i=0}^{L-m-2i \geq 0} \zeta(\beta; i, m, L) / \xi(i, m, L)$ (where $\zeta(\beta; i, m, L) = \left((1-2\beta^2)^{\frac{L-m-2i}{2}} \beta^{m+2i} \right)^2 L!$ and $\xi(i, m, L) = (L-m-2i)!(m+2i)!$) is Gaussian with mean $L \cdot n^{\text{ph}}$ and encompasses the phonon sectors $N_m^{\text{ph}} = Ln + m$, with $m = -L, -L+1, \dots, +L-1, +L$ (see supplemental materials [56]). In Fig. 4a we compare the post-pump dynamics following the application of \hat{A}^c with that obtained following the application of \hat{A}^{sc} for pump fluence corresponding to exciting $n^{\text{ph}} = 1, 4$ phonons locally on each site. Notably, the ensuing dynamics for the two pulse shapes are nearly identical. Examining the global phonon distribution $\mathcal{P}(N^{\text{ph}})$ for both types of pulses (middle inset of Fig. 4a) we find good agreement within the error bars. This suggests that manipulating the local onsite phonon distribution created by the pump bears no effect on the electronic dynamics while tuning the global phonon distribution $\mathcal{P}(N^{\text{ph}})$ may allow better control at least over short and intermediate timescales. This is what we find in Fig. 4b where we show the dynamics following the application of various β pulses corresponding to global phonon distribution with varied width $\sigma(\beta)$. Here, we observe a strong correlation between increasing the value of σ and generating a larger light-induced double occupancy.

Conclusion. We introduced PST as a tool to decompose the fully coupled electron-phonon wavefunction into

electronic contributions weighted by phonon occupations, which can be sampled efficiently to reconstruct electronic observables. We demonstrate the usefulness of PST by simulating the experimental protocol for probing the phononic response of a metal whose phonons are excited by a pump pulse at an initial time, obtaining sample-averaged phonon occupations that can be matched to experiments and accurately reconstructing the dynamics of electronic correlations. PST thus enables building a connection between phononic observables measured in direct phonon probes and the underlying electronic correlations, which may be relevant to experiments based on diffuse x-ray and electron scattering. We also show how to use PST to analyze and design different pulse shapes tailored to enhance or suppress certain electronic correlations in the post-pump dynamics. PST may thus aid in the experimental control of light-matter interaction and the analysis of experimental data.

Acknowledgements M. Mor., U. S., and S. P. acknowledge support by the Deutsche Forschungsgemeinschaft (DFG, German Research Foundation) under Germany's Excellence Strategy-426 EXC-2111-390814868. M. Mit. acknowledges support by the U.S. Department of Energy, Office of Basic Energy Sciences, Early Career Award Program, under Award No. DE-SC0022883.

* Author to whom correspondence should be address; sebastian.paeckel@physik.uni-muenchen.de. These authors contributed equally and are listed alphabetically.

† Author to whom correspondence should be address; jsous@ucsd.edu. These authors contributed equally and are listed alphabetically.

- [1] D. Fausti, R. I. Tobey, N. Dean, S. Kaiser, A. Dienst, M. C. Hoffmann, S. Pyon, T. Takayama, H. Takagi, and A. Cavalleri, *Science* **331**, 189 (2011).
- [2] M. Mitrano, A. Cantaluppi, D. Nicoletti, S. Kaiser, A. Perucchi, S. Lupi, P. Di Pietro, D. Pontiroli, M. Riccò, S. R. Clark, D. Jaksch, and A. Cavalleri, *Nature* **530**, 461 (2016).
- [3] A. Cantaluppi, M. Buzzi, G. Jotzu, D. Nicoletti, M. Mitrano, D. Pontiroli, M. Riccò, A. Perucchi, P. Di Pietro, and A. Cavalleri, *Nat. Phys.* **14**, 837 (2018).
- [4] S. Biswas, J. Husek, and L. R. Baker, *Chem. Commun.* **54**, 4216 (2018).
- [5] L. Schwarz and D. Manske, *Phys. Rev. B* **101**, 184519 (2020).
- [6] C. Clear, R. C. Schofield, K. D. Major, J. Iles-Smith, A. S. Clark, and D. P. S. McCutcheon, *Phys. Rev. Lett.* **124**, 153602 (2020).
- [7] M. Budden, T. Gebert, M. Buzzi, G. Jotzu, E. Wang, T. Matsuyama, G. Meier, Y. Laplace, D. Pontiroli, M. Riccò, F. Schlawin, D. Jaksch, and A. Cavalleri, *Nat. Phys.* **17**, 611 (2021).
- [8] M. Buzzi, G. Jotzu, A. Cavalleri, J. I. Cirac, E. A. Demler, B. I. Halperin, M. D. Lukin, T. Shi, Y. Wang, and D. Podolsky, *Phys. Rev. X* **11**, 011055 (2021).

- [9] D. Campi, S. Kumari, and N. Marzari, *Nano Lett.* **21**, 3435 (2021), publisher: American Chemical Society.
- [10] Y. H. Wang, H. Steinberg, P. Jarillo-Herrero, and N. Gedik, *Science* **342**, 453 (2013).
- [11] F. Mahmood, C.-K. Chan, Z. Alpichshev, D. Gardner, Y. Lee, P. A. Lee, and N. Gedik, *Nat. Phys.* **12**, 306 (2016).
- [12] J.-Y. Shan, M. Ye, H. Chu, S. Lee, J.-G. Park, L. Balents, and D. Hsieh, *Nature* **600**, 235 (2021).
- [13] S. Zhou, C. Bao, B. Fan, H. Zhou, Q. Gao, H. Zhong, T. Lin, H. Liu, P. Yu, P. Tang, S. Meng, W. Duan, and S. Zhou, *Nature* **614**, 75 (2023).
- [14] M. Rini, R. Tobey, N. Dean, J. Itatani, Y. Tomioka, Y. Tokura, R. W. Schoenlein, and A. Cavalleri, *Nature* **449**, 72 (2007).
- [15] M. Först, C. Manzoni, S. Kaiser, Y. Tomioka, Y. Tokura, R. Merlin, and A. Cavalleri, *Nat. Phys.* **7**, 854 (2011).
- [16] A. Subedi, A. Cavalleri, and A. Georges, *Phys. Rev. B* **89**, 220301 (2014).
- [17] T. F. Nova, A. Cartella, A. Cantaluppi, M. Först, D. Bossini, R. V. Mikhaylovskiy, A. V. Kimel, R. Merlin, and A. Cavalleri, *Nat. Phys.* **13**, 132 (2017).
- [18] A. S. Disa, T. F. Nova, and A. Cavalleri, *Nat. Phys.* **17**, 1087 (2021).
- [19] G. Khalsa, N. A. Benedek, and J. Moses, *Phys. Rev. X* **11**, 021067 (2021).
- [20] M. Henstridge, M. Först, E. Rowe, M. Fechner, and A. Cavalleri, *Nat. Phys.* **18**, 457 (2022).
- [21] J. Sous, B. Kloss, D. M. Kennes, D. R. Reichman, and A. J. Millis, *Nat. Commun.* **12**, 5803 (2021).
- [22] M. Knap, M. Babadi, G. Refael, I. Martin, and E. Demler, *Phys. Rev. B* **94**, 214504 (2016).
- [23] M. Babadi, M. Knap, I. Martin, G. Refael, and E. Demler, *Phys. Rev. B* **96**, 014512 (2017).
- [24] D. M. Kennes, E. Y. Wilner, D. R. Reichman, and A. J. Millis, *Nat. Phys.* **13**, 479 (2017).
- [25] D. M. Kennes, E. Y. Wilner, D. R. Reichman, and A. J. Millis, *Phys. Rev. B* **96**, 054506 (2017).
- [26] Y. Murakami, N. Tsuji, M. Eckstein, and P. Werner, *Phys. Rev. B* **96**, 045125 (2017).
- [27] H. Hübener, U. De Giovannini, and A. Rubio, *Nano Lett.* **18**, 1535 (2018).
- [28] S. Paeckel, B. Fauseweh, A. Osterkorn, T. Köhler, D. Manske, and S. R. Manmana, *Phys. Rev. B* **101**, 180507 (2020).
- [29] C. J. Eckhardt, S. Chattopadhyay, D. M. Kennes, E. A. Demler, M. A. Sentef, and M. H. Michael, “Theory of resonantly enhanced photo-induced superconductivity,” (2023), [arXiv:2303.02176](https://arxiv.org/abs/2303.02176) [[cond-mat.supr-con](https://arxiv.org/abs/2303.02176)].
- [30] M. Trigo, J. Chen, V. H. Vishwanath, Y. M. Sheu, T. Graber, R. Henning, and D. A. Reis, *Phys. Rev. B* **82**, 235205 (2010).
- [31] M. Trigo, M. Fuchs, J. Chen, M. P. Jiang, M. Cammarata, S. Fahy, D. M. Fritz, K. Gaffney, S. Ghimire, A. Higginbotham, S. L. Johnson, M. E. Kozina, J. Larson, H. Lemke, A. M. Lindenberg, G. Ndashimiye, F. Quirin, K. Sokolowski-Tinten, C. Uher, G. Wang, J. S. Wark, D. Zhu, and D. A. Reis, *Nat. Phys.* **9**, 790 (2013).
- [32] T. Konstantinova, J. D. Rameau, A. H. Reid, O. Abdu-razakov, L. Wu, R. Li, X. Shen, G. Gu, Y. Huang, L. Rettig, I. Avigo, M. Ligges, J. K. Freericks, A. F. Kemper, H. A. Dürr, U. Bovensiepen, P. D. Johnson, X. Wang, and Y. Zhu, *Sci. Adv.* **4**, eaap7427 (2018).
- [33] T. Köhler, J. Stolpp, and S. Paeckel, *SciPost Phys.* **10** (2021).
- [34] J. Stolpp, T. Köhler, S. R. Manmana, E. Jeckelmann, F. Heidrich-Meisner, and S. Paeckel, *Comput. Phys. Commun.* **269**, 108106 (2021).
- [35] W. Hu, S. Kaiser, D. Nicoletti, C. R. Hunt, I. Gierz, M. C. Hoffmann, M. Le Tacon, T. Loew, B. Keimer, and A. Cavalleri, *Nat. Mater.* **13**, 705 (2014).
- [36] S. Kaiser, C. R. Hunt, D. Nicoletti, W. Hu, I. Gierz, H. Y. Liu, M. Le Tacon, T. Loew, D. Haug, and B. Keimer, *Phys. Rev. B* **89**, 184516 (2014).
- [37] M. Buzzi, D. Nicoletti, M. Fechner, N. Tancogne-Dejean, M. A. Sentef, A. Georges, T. Biesner, E. Uykur, M. Dreschel, A. Henderson, T. Siegrist, J. A. Schlueter, K. Miyagawa, K. Kanoda, M.-S. Nam, A. Ardavan, J. Coulthard, J. Tindall, F. Schlawin, D. Jaksch, and A. Cavalleri, *Phys. Rev. X* **10**, 031028 (2020).
- [38] M. Fechner, M. Först, G. Orenstein, V. Krapivin, A. S. Disa, M. Buzzi, A. von Hoegen, G. de la Pena, Q. L. Nguyen, R. Mankowsky, M. Sander, H. Lemke, Y. Deng, M. Trigo, and A. Cavalleri, *Nat. Mater.* (2024).
- [39] A. S. Disa, J. Curtis, M. Fechner, A. Liu, A. von Hoegen, M. Först, T. F. Nova, P. Narang, A. Maljuk, A. V. Boris, B. Keimer, and A. Cavalleri, *Nature* **617**, 73 (2023).
- [40] B. Liu, M. Först, M. Fechner, D. Nicoletti, J. Porras, T. Loew, B. Keimer, and A. Cavalleri, *Phys. Rev. X* **10**, 011053 (2020).
- [41] E. Rowe, B. Yuan, M. Buzzi, G. Jotzu, Y. Zhu, M. Fechner, M. Först, B. Liu, D. Pontiroli, M. Riccò, and A. Cavalleri, *Nat. Phys.* (2023).
- [42] R. Mankowsky, A. Subedi, M. Först, S. O. Mariager, M. Chollet, H. T. Lemke, J. S. Robinson, J. M. Glowia, M. P. Minitti, A. Frano, M. Fechner, N. A. Spaldin, T. Loew, B. Keimer, A. Georges, and A. Cavalleri, *Nature* **516**, 71 (2014).
- [43] R. Mankowsky, M. Först, T. Loew, J. Porras, B. Keimer, and A. Cavalleri, *Phys. Rev. B* **91**, 094308 (2015).
- [44] R. Xu and T. C. Chiang, *Z. Kristallogr. – Cryst. Mater.* **220**, 1009 (2005).
- [45] S. R. White, *Phys. Rev. Lett.* **69**, 2863 (1992).
- [46] S. R. White, *Phys. Rev. B* **48**, 10345 (1993).
- [47] U. Schollwöck, *Rev. Mod. Phys.* **77**, 259 (2005).
- [48] U. Schollwöck, *Ann. Phys.* **326**, 96 (2011).
- [49] A. Bohrdt, C. S. Chiu, G. Ji, M. Xu, D. Greif, M. Greiner, E. Demler, F. Grusdt, and M. Knap, *Nat. Phys.* **15**, 921 (2019).
- [50] A. Bohrdt, S. Kim, A. Lukin, M. Rispoli, R. Schittko, M. Knap, M. Greiner, and J. Léonard, *Phys. Rev. Lett.* **127**, 150504 (2021).
- [51] A. Bohrdt, L. Homeier, C. Reinmoser, E. Demler, and F. Grusdt, *Ann. Phys.* **435**, 168651 (2021).
- [52] M. Buser, U. Schollwöck, and F. Grusdt, *Phys. Rev. A* **105** (2022).
- [53] F. A. Palm, S. Mardazad, A. Bohrdt, U. Schollwöck, and F. Grusdt, *Phys. Rev. B* **106**, L081108 (2022).
- [54] F. J. Paww, F. A. Palm, U. Schollwöck, A. Bohrdt, S. Paeckel, and F. Grusdt, “Detecting hidden order in fractional chern insulators,” (2023), [arXiv:2309.03666](https://arxiv.org/abs/2309.03666) [[cond-mat.quant-gas](https://arxiv.org/abs/2309.03666)].
- [55] S. Hirthe, T. Chalopin, D. Bourgund, P. Bojović, A. Bohrdt, E. Demler, F. Grusdt, I. Bloch, and T. A. Hilker, *Nature* **613**, 463 (2023).
- [56] Supplemental Material. Link to be added.

- [57] R. Mankowsky, M. Först, and A. Cavalleri, [Rep. Prog. Phys.](#) **79**, 064503 (2016).
- [58] J. Haegeman, J. I. Cirac, T. J. Osborne, I. Pižorn, H. Verschelde, and F. Verstraete, [Phys. Rev. Lett.](#) **107**, 070601 (2011).
- [59] J. Haegeman, C. Lubich, I. Oseledets, B. Vandereycken, and F. Verstraete, [Phys. Rev. B](#) **94**, 165116 (2016).
- [60] S. Paeckel, T. Köhler, A. Swoboda, S. R. Manmana, U. Schollwöck, and C. Hubig, [Ann. Phys.](#) **411**, 167998 (2019).
- [61] M. Yang and S. R. White, [Phys. Rev. B](#) **102**, 094315 (2020).
- [62] M. Yang and S. R. White, [Phys. Rev. B](#) **102** (2020).